Pentagonal Bipyramidal 3 d-Metal Complexes Derived from a Dimethylcarbamoyl-Substituted Pentadentate-[N 3 O 2] Ligand: Aiming for Increased Solubility

Valentin Jubault, François Genevois, Barthélémy Pradines, Benjamin Cahier, Wejden Jbeli, Nicolas Suaud, Nathalie Guihéry, Carine Duhayon, Céline Pichon, Jean-pascal Sutter

ChemistrySelect

Research Article
doi.org/10.1002/slct.202204935

Chemistry Europe
European Chemical Societies Publishing

www.chemistryselect.org

Pentagonal Bipyramidal 3 d-Metal Complexes Derived from a Dimethylcarbamoyl-Substituted Pentadentate-$[N_3O_2]$ Ligand: Aiming for Increased Solubility

Valentin Jubault,[a] François Genevois,[a] Barthélémy Pradines,[b] Benjamin Cahier,[b] Wejden Jbeli,[a, c] Nicolas Suaud,[b] Nathalie Guihéry,[b] Carine Duhayon,[a] Céline Pichon,[a] and Jean-Pascal Sutter*[a]

A pentadentate-$[N_3O_2]$ ligand, H_2L^{NMe2}, formed by condensation of diacetyl pyridine and dimethylcarbamoyl hydrazide (i.e. $Me_2NCONHNH_2$), is reported to yield mononuclear pentagonal bipyramidal (PBP) metal complexes with Cr^{III}, Mn^{II}, Fe^{II}, Co^{II}, and Ni^{II}, that exhibit good solubility in a wide range of solvents as compared to the classically used H_2L^R ligands. With Cu^{II}, dinuclear complexes were obtained. The potassium salt of the deprotonated ligand, K_2L^{NMe2}, was also characterized. The reported complexes consist of $[CrH_2L^{NMe2}Cl_2]\cdot Cl$; $Cat[CrL^{NMe2}(CN)_2]$ ($Cat = K^+$ or PNP^+); $[MH_2L^{NMe2}(H_2O)_2]\cdot(ClO_4)_2$ with $M = Mn^{II}$, Co^{II}, or Ni^{II}; $[FeH_2L^{NMe2}(MeCN)_2]\cdot(PF_6)_2\cdot MeCN$; $[FeH_2L^{NMe2}(MeOH)X]\cdot X$ ($X = Br$ or I); $[\{CuH_2L^{NMe2}\}_2(MeOH)(ClO_4)]\cdot(ClO_4)_3\cdot 1H_2O\cdot 1.75H_2O$; $[CuHL^{NMe2}]_2\cdot(ClO_4)_2\cdot H_2O$; and $[CuH_2L^{NMe2}(H_2O)]_2\cdot(ClO_4)_4\cdot 5H_2O$. The magnetic behaviors of the PBP derivatives were assessed, especially the zero-field splitting (ZFS) characteristics for the Cr^{III}, Fe^{II}, Co^{II}, and Ni^{II} derivatives. The ZFS characteristics were also determined from *ab initio* theoretical calculations. The obtained values confirm those extracted from magnetic measurements.

Introduction

Magnetic anisotropy plays an important role in the behavior of magnetic materials. For instance, the hardness (i.e. coercive field) of bulk magnets is mainly proportional to the magnetic anisotropy; the energy barrier for the reversal of magnetization of molecular nanomagnets such as Single-Molecule Magnets (SMM) and Single-Chain Magnets (SCM) greatly relies on large axial anisotropy; and the operation of molecular Spin Qubits necessitates a weak in-plan magnetic anisotropy. The design of such materials therefore requires a perfect control of the magnetic anisotropy of individual magnetic centers, which depends on various parameters such as the nature of the metal ion and its electronic configuration, as well as its coordination geometry.[1–2]

For molecule-based materials assembled from molecular fragments, these features can be defined in the preformed building units, thereby imparting controlled magnetic anisotropy to the magnetic centers of the targeted system. In this context, seven-coordinated 3d ion complexes with pentagonal bipyramidal (PBP) geometry are of great relevance as building blocks. This coordination geometry allows easy access to a wide range of axial or planar magnetic anisotropy that depends mainly on the electronic configuration of the metal ion. Thus, small or large Zero-Field Splitting (ZFS) D values (up to about $\pm 30\ cm^{-1}$) with a positive or negative sign can be rationally obtained simply by selecting the appropriate metal center.[3] Furthermore, PBP complexes based on a pentadentate equatorial ligand are robust enough to allow substitutions at the apical positions without compromising the coordination geometry and, consequently, the magnetic anisotropy. The latter complexes are particularly suitable for the formation of 1D coordination polymers as illustrated by the preparation of several SCMs.[4–10] However, chain systems are not systematically the result of these associations; frequently smaller polynuclear compounds are crystallized. Based on our experience with PBP complexes formed with the pentadentate ligand H_2L^R (Scheme 1, $R = NH_2$, Ph, alkyl, etc.), we suggested that the peripheral R-group plays an important role in the outcome of the assembly process,[11] which can be attributed to solubility considerations of the oligomeric species formed during the assembly process. The same argument also applies to the solubility of these PBP metal complexes in various solvents. We therefore considered a ligand, i.e. the substituent R, which would lead to good solubility of the metal complexes in common solvents without being intrusive and changing the coordination characteristics of the ligand. Herein we report that these conditions are met for $R = NMe_2$.

[a] *Dr. V. Jubault, F. Genevois, W. Jbeli, Dr. C. Duhayon, Dr. C. Pichon, Dr. J.-P. Sutter*
Laboratoire de Chimie de Coordination du CNRS (LCC), Université de Toulouse, CNRS, F-31077 Toulouse, France
E-mail: jean-pascal.sutter@lcc-toulouse.fr
Homepage: https://www.lcc-toulouse.fr/
[b] *Dr. B. Pradines, Dr. B. Cahier, Dr. N. Suaud, Prof. Dr. N. Guihéry*
Laboratoire de Chimie et Physique Quantiques (LCPQ), Université de Toulouse, CNRS, 118 route de Narbonne, F-31062 Toulouse, France
[c] *W. Jbeli*
University of Tunis El Manar, Faculty of Sciences of Tunis, Laboratory of Materials, Crystal Chemistry and Applied Thermodynamics, 2092 El Manar II, Tunis, Tunisia

Supporting information for this article is available on the WWW under https://doi.org/10.1002/slct.202204935

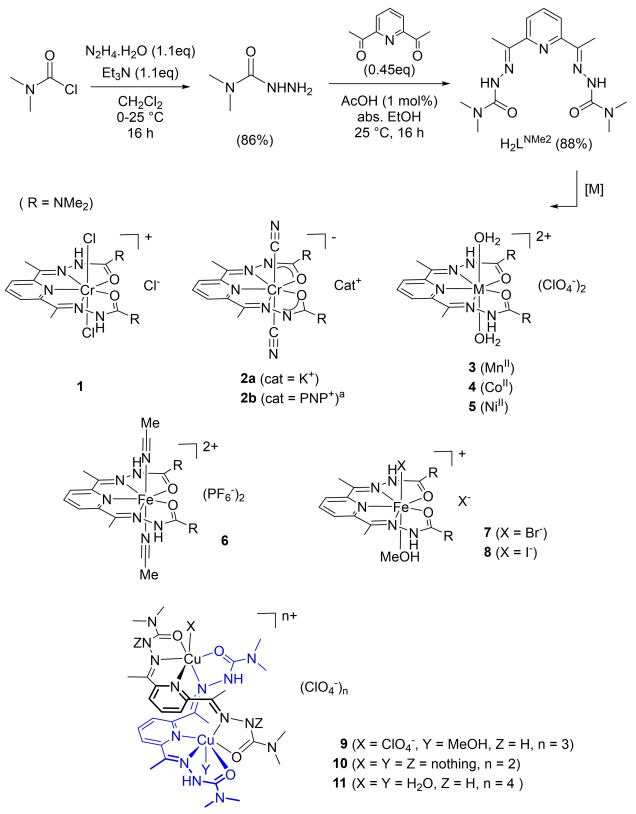

Scheme 1. Synthesis pathway to H_2L^{NMe2} and reported complexes. [a] PNP^+ stands for bis(triphenylphosphine)iminium.

Several metal complexes (Cr^{III}, Mn^{II}, Fe^{II}, Co^{II}, Ni^{II}, and Cu^{II}) have been prepared to confirm the coordination features of the ligand, and the magnetic behaviors of the PBP derivatives were assessed, especially the ZFS characteristics. The ZFS characteristics have also been examined from a theoretical view point. The potassium salt of the deprotonated ligand, K_2L^{NMe2}, was characterized; this reagent was involved in the synthesis of the dicyanido complex $[CrL^{NMe2}(CN)_2]^-$.

Results and Discussion

Synthesis

The ligand H_2L^{NMe2} was prepared in high yield as outlined in Scheme 1, details can be found in the experimental section.[12] During the synthesis of the dimethylcarbamoyl hydrazide, a small amount (1-3%) of a by-product was systematically observed by ^1H NMR (singulet at $\delta = 2.97$ ppm in $CDCl_3$) which is tentatively assigned to bis-substituted N,N′-bis(dimethylcarbamoyl) hydrazide. This impurity was found even when a larger excess of hydrazine was used but since it cannot interfere in the second step of the synthesis, the condensation with diacetylpyridine was performed without further purification, giving H_2L^{NMe2} with about 90% yield. It can be mentioned that the latter reaction must be performed at room temperature to avoid the formation of side products.

The reaction of H_2L^{NMe2} and two equivalents of ^{t}BuOK in anhydrous THF gave the dianionic ligand salt $[K_2L^{NMe2}]$. Yellow-orange needles of $K_2L^{NMe2}\cdot 2THF$ were formed in the reaction mixture, allowing the structural characterization of this compound.

$[CrH_2L^{NMe2}Cl_2]\cdot Cl$, **1**, *and Cat$[CrL^{NMe2}(CN)_2]$*, **2a**,**b** *(Cat = K^+ and PNP^+, respectively)*: Complex **1** was isolated from the reaction of H_2L^{NMe2} and $CrCl_3.6H_2O$ in MeOH upon addition of Et_2O. This is a rare example of Cr^{III} of PBP geometry with a neutral H_2L^R ligand;[13] in general ligand deprotonation is concomitant with Cr coordination.[14–15] Unsurprisingly, X-ray powder diffraction data indicated that **1** is not the sole product of the reaction (Figure S14), suggesting that a deprotonated complex was also formed. No attempts were made to obtain **1** in pure form because this mixture of Cr complexes was involved in a reaction with an excess of cyanides, acting as ligands and base, to obtained the para dicyanido complex $[CrL^{NMe2}(CN)_2]^-$. A more rational synthesis of $[CrL^{NMe2}(CN)_2]^-$ consisted in the deprotonation of H_2L^{NMe2} with ^{t}BuOK prior to complexation with $CrCl_3(THF)_3$, and subsequently addition of the CN^- ligands. This led to the potassium salt **2a** which appeared difficult to purify and very hygroscopic. The same reaction sequence gave **2b** with about 68% yield after cation exchange for bis(triphenylphosphine)iminium (PNP^+). The latter compound was found to be soluble in MeOH, EtOH, CH_2Cl_2, $CHCl_3$, and MeCN. It crystallized easily by diffusion of Et_2O into a solution in MeCN, CH_2Cl_2, or $CHCl_3$, forming the same crystallographic phase. The IR signal characteristic for ν_{CN} was found at 2132 cm^{-1} for **2a** and at 2127 and 2119 cm^{-1} for **2b**; these bands are weak (Figures in SI).

$[MH_2L^{NMe2}(H_2O)_2]\cdot(ClO_4)_2$, **3**–**5**: The complexes with M = Mn^{II} (**3**), Co^{II} (**4**), or Ni^{II} (**5**) were obtained reacting H_2L^{NMe2} and the corresponding perchlorate salt in MeOH/H_2O (1/1) solution; crystals were formed by slow evaporation of the solvent.

$[FeH_2L^{NMe2}(MeCN)_2]\cdot(PF_6)_2\cdot MeCN$, **6**: This complex was synthesized in oxygen-free conditions from anhydrous $FeCl_2$ in acetonitrile in the presence of NH_4PF_6. The IR of a solid sample showed three bands at 2297, 2263, and 2252 cm^{-1} attributed to MeCN; the last two can be assigned to lattice solvent molecules[16] and that of highest energy to the coordinated acetonitriles. A temporal follow-up by infrared showed their strongly labile character, whether co-crystallized or coordinated. All three bands disappeared within a few minutes with the concomitant emergence of a band at 3637 cm^{-1} suggesting an exchange with H_2O from air (see Figure S15).

$[FeH_2L^{NMe2}(MeOH)X]\cdot X$, **7** (X = Br) and **8** (X = I): The complex $[FeH_2L^{NMe2}(MeOH)Br]\cdot Br$, **7**, was prepared by reaction of H_2L^{NMe2} with anhydrous $FeBr_2$ in MeOH whereas the homologous complex $[FeH_2L^{NMe2}(MeOH)I]\cdot I$, **8**, was obtained by halogen exchange from the chloro-complex. The complex with X = Cl could not be crystallized; therefore it is not discussed herein.

Several attempts were made to obtained PBP Cu^{II} complexes but only binuclear derivatives with penta- or hexa-coordinated Cu centers were isolated (i.e. $[\{CuH_2L^{NMe2}\}_2(MeOH)(ClO_4)]\cdot(ClO_4)_3\cdot 1H_2O\cdot 1.75H_2O$, **9**; $[CuHL^{NMe2}]_2\cdot(ClO_4)_2\cdot H_2O$, **10**; and $[CuH_2L(H_2O)]_2\cdot(ClO_4)_4\cdot 5H_2O$, **11**). Details of the reaction conditions can be found in the

experimental section (see SI). In **10**, each pentadentate ligand is singly deprotonated, which is clearly reflected by the IR spectrum that shows split bands, in particular for the CO and the CN vibrations (1642/1635 and 1540/1535 cm^{-1}).

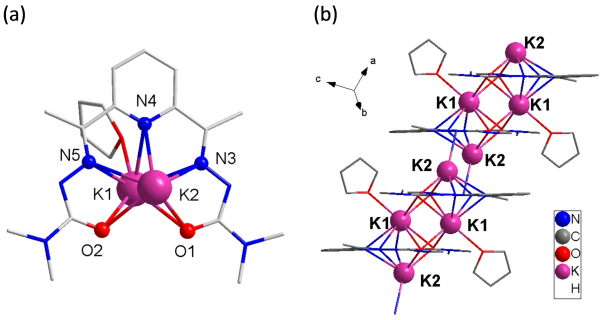

Figure 1. $[K_2(THF)L^{NMe2}]$·THF: (a) Molecular structure and (b) supramolecular organization. Hydrogen atoms and lattice THF are not depicted.

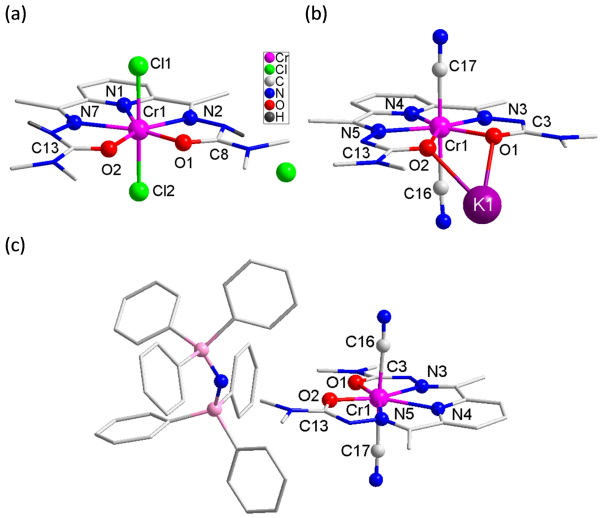

Figure 2. Molecular structures of the Cr complexes **1** (a), **2a** (b), and **2b** (c) with their counter-ions. Lattice solvent molecules and H-atoms are not shown except the H of the N-hydrazide moieties in **1**.

Crystal structures

The crystal structures for all the metal complexes have been solved. General crystallographic information are gathered in Table S1 and S2 in the Supporting Information where plots with atoms labels and selected bond distances and angles can be found for each structure.

The compound $K_2L^{NMe2}.2THF$ crystallized in the triclinic space group *P*-1. It consists in a 1D coordination polymer made up by two K^+, one $[L^{NMe2}]^{2-}$, and one THF molecule, an additional THF being located in the lattice. The $[L^{NMe2}]^{2-}$ unit is flat with N–N–C(O) angles of 109.1 and 109.4°, in agreement with deprotonated hydrazide moieties.[3] The potassium ions are located above and below the cavity of $[L^{NMe2}]^{2-}$ ligand to which they are bound by κ^5-N_3O_2 chelating coordination. The K^+ ions also coordinate to O- and N-atoms of neighboring $[K_2L^{NMe2}]$ units, thus developing the 1D-organization depicted in Figure 1. The coordinated THF molecule is bonded to K1, the second is located between the $[K_2(THF)(L^{NMe2})]$ arrays.

The molecular structure for $[CrH_2L^{NMe2}Cl_2]\cdot Cl\cdot MeOH\cdot 0.5H_2O$, **1**, $K[CrL^{NMe2}(CN)_2]$, **2a**, and $PNP[CrL^{NMe2}(CN)_2]$, **2b** are shown in Figure 2. These complexes crystallized in the triclinic space group *P*-1. Their structure corresponds to heptacoordinate Cr^{III} center with PBP geometry. The equatorial plane consists of three N and two O atoms of the neutral H_2L^{NMe2} for **1**, or dianionic $[L^{NMe2}]^{2-}$ ligand, for **2a**,**b**, while the apical positions are respectively occupied by two chloride or two cyanido groups. In the pentadentate ligands, the hydrazide moieties have N–N-C(O) angles (Table 1) above in **1**, and below in **2a**,**b**, the 110° threshold angle distinguishing protonated from deprotonated hydrazide groups in this type of ligand.[3] These geometrical parameters confirm the occurrence of the ligand in its neutral form, H_2L^{NMe2}, in **1** and its dianionic form, $[L^{NMe2}]^{2-}$, in **2a**,**b**. Complex **1** is therefore monocationic and its charge is balanced by a chloride ion; it crystallized with one MeOH and 0.5 H_2O lattice molecules. Compounds **2a**,**b** are monoanionic and their charge is balanced by one K^+ or PNP^+ ion, respectively. The metal-ligand bond lengths of the first coordination sphere are given in Table 1. It can be noticed that in **2a** the equatorial Cr–O bond distances are significantly larger as in the other two complexes, a feature that can be ascribed to the interactions of the same O atoms with the K^+ ions. Likewise, the Cr–CN arrangement is slightly bent (171.7°) due to an obvious interaction of the π-electron cloud of the C≡N group with

Table 1. Coordination bond lengths (Å) and angles (°) for **1**, **2a**, and **2b**.

1		**2a**		**2b**	
Cr1–N1	2.347(2)	Cr1–N4	2.024(3)	Cr1–N4	2.403(1)
Cr1–N2	2.173(2)	Cr1–N3	2.062(4)	Cr1–N3	2.264(1)
Cr1–N7	2.287(2)	Cr1–N5	2.149(4)	Cr1–N5	2.203(1)
Cr1–O2	2.010(2)	Cr1–O2	2.467(3)	Cr1–O1	1.978(1)
Cr1–O1	1.990(2)	Cr1–O1	2.127(3)	Cr1–O2	1.972(1)
Cr1–Cl2	2.315(1)	Cr1–C16	2.094(3)	Cr1–C17	2.093(2)
Cr1–Cl1	2.316(1)	Cr1–C17	2.047(3)	Cr1–C16	2.108(1)
Cl2–Cr1–Cl1	176.05(3)	C16–Cr1–C17	173.8(2)	C17–Cr1–C16	176.09(5)
N2–N3–C8	111.7(2)	N3–N2–C3	107.9(3)	N3–N2–C3	107.5(1)
N7–N6–C13	112.0(2)	N5–N6–C13	110.0(3)	N5–N6–C13	107.9(1)

potassium. Such bending is no longer observed in **2b**. The shortest intermolecular M···M distances are 9.342, 9.206 and 12.961 Å for **1**, **2a**, and **2b**.

In the three complexes the Cr centers exhibit PBP coordination polyhedra. Distortion from the ideal geometry was evaluated with SHAPE software[17] and given by the deviance from zero of the CShM values[18] for the PBP-7[19] and PP-5[20] (equatorial plane) geometries. Values of respectively (PBP-7/PP-5) 0.358/0.247, 0.261/0.270, and 0.330/0.290 have been found for **1**, **2a**, and **2b**, confirming PBP coordination spheres and slightly distorted equatorial arrangements.

The complexes $[MH_2L^{NMe2}(H_2O)_2]\cdot(ClO_4)_2$ with M = Mn^{II} (**3**), Co^{II} (**4**), or Ni^{II} (**5**) crystallized in the orthorhombic space group *Pbca* for **3** and **4**, and in the monoclinic group $P2_1/n$ for **5**. Their molecular complexes are isomorphous; each consists in a heptacoordinate M^{2+} center of slightly distorted PBP geometry (Figure 3). The equatorial plane is constituted by three N and two O atoms of the pentadentate ligand H_2L^{NMe2} and the two apical positions are occupied by H_2O molecules. For all complexes the hydrazide moieties have N–N–C(O) angles above 110° (Table 2) confirming that the pentadentate ligand is involved in its neutral form. The charge of the dicationic complex is compensated by two ClO_4^- anions. The metal-ligand bond lengths of the first coordination sphere of each derivative and some angles are given in Table 2. It is noticed that Mn^{II} and Co^{II} ions adopt an almost symmetrically position in the $[N_3O_2]$ pentagonal plane; this is not the case for Ni^{II}. In **5**, significantly different bond distances are found with the two imino-nitrogen atoms, N3 and N5, and even more for the carbonyl-oxygen atoms, the Ni–O1 bond reaching 2.51 Å. This is not unusual in PBP Ni complexes and can be attributed to the smaller ionic radius of Ni^{II}, and the Jahn-Teller effect that applies for this ion.[21–24] However, SHAPE calculations revealed that the coordination sphere in **5** only slightly deviates from ideal PBP with CShM value of 0.47 compared with 1.00 for **3** and 0.74 for **4**. The larger deviation for the last two complexes is related to a distortion of the equatorial coordination arrangements that significantly deviate from planar pentagonal (CShM versus PP-5 of respectively 1.27 and 0.91). For **3** and **4**, the O atoms of the ligand (i.e. O1 and O2 in Figure 3) are positioned slightly above and below the plane defined by the three N-atoms linked to the metal center.

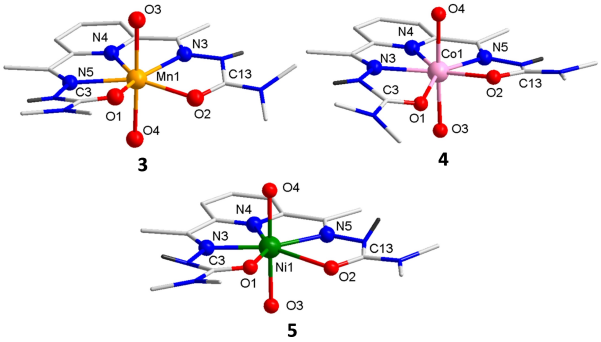

Figure 3. Molecular structures of $[MH_2L^{NMe2}(H_2O)_2]\cdot(ClO_4)_2$ with M = Mn^{II} (**3**), Co^{II} (**4**), or Ni^{II} (**5**). The counter-ions and H atoms are not shown except the H of the N-hydrazide moieties.

When comparing these complexes with related compounds of general formulation $[M(H_2L^R)XY]Z$, it is apparent that Co^{II} and Mn^{II} derivatives **3** and **4** have some of the shortest metal-ligand bonds while for **5** they are similar to those found in PBP Ni complexes (see Table S3). These shorter bond lengths result in a more compressed equatorial coordination sphere, which may explain the deformations in **3** and **4**.

The compounds $[FeH_2L^{NMe2}(MeCN)_2]\cdot(PF_6)_2\cdot MeCN$, **6**, $[FeH_2L^{NMe2}(MeOH)Br]\cdot Br$, **7**, and $[FeH_2L^{NMe2}(MeOH)I]\cdot I$, **8**, crystallized in the monoclinic space group $P2_1/c$. Each of these molecular complexes consists in a Fe^{II} center with PBP coordination sphere (Figure 4). The equatorial plane accommodates three N and two O atoms of a neutral H_2L^{NMe2} (the hydrazide N–N–C(O) angles are above 110°, Table 3) while the apical positions are occupied by two MeCN for **6**, MeOH and Br for **7**, and MeOH and I for **8**. The dicationic charge of complex **6** is compensated by two PF_6^- anions; and a MeCN is located in the crystal lattice. Complexes **7** and **8** are monocationic and their charge is compensated by a bromide and iodide ion, respectively.

Evaluation with SHAPE of the coordination sphere distortion from the ideal PBP geometry yielded CShM values of 0.164, 0.792, and 1.237, respectively for complexes **6**–**8**. For these complexes, the apparent deviation from a PBP geometry is not due to a non-planarity of the equatorial coordination sphere as for complexes **3** and **4**; here, all the atoms involved lie in a pentagonal plane (CShM values versus PP-5 are 0.12, 0.22, and 0.21, respectively from **6** to **8**). The increasing distortion of the PBP shape is due to the elongation of the apical bond following the increase in the atomic radius of the coordinated atom (N <

Table 2. Selected bond lengths (Å) and angles (°) for **3**–**5**.

3		**4**		**5**	
Mn1–N3	2.295(2)	Co1–N3	2.190(2)	Ni1–N3	2.093(2)
Mn1–N4	2. 290(2)	Co1–N4	2.184(2)	Ni1–N4	2. 023(2)
Mn1–N5	2.288(2)	Co1–N5	2.186(2)	Ni1–N5	2.186(2)
Mn1–O1	2.191(1)	Co1–O1	2.188(1)	Ni1–O1	2.247(2)
Mn1–O2	2.221(2)	Co1–O2	2. 144(1)	Ni1–O2	2.511(2)
Mn1–O4	2. 235(1)	Co1–O3	2.158(1)	Ni1–O3	2.041(2)
Mn1–O3	2.215(2)	Co1–O4	2.151(2)	Ni1–O4	2.0.57(3)
O4–Mn1–O3	178.54(5)	O3–Co1–O4	176.47(5)	O3–Ni1–O4	173.72(9)
N3–N2–C13	113.1(2)	N3–N2–C3	112.6(2)	N3–N29–C3	113.5(2)
N5–N6–C3	114.2(2)	N5–N6–C13	113.4(2)	N5–N69–C13	114.1(2)

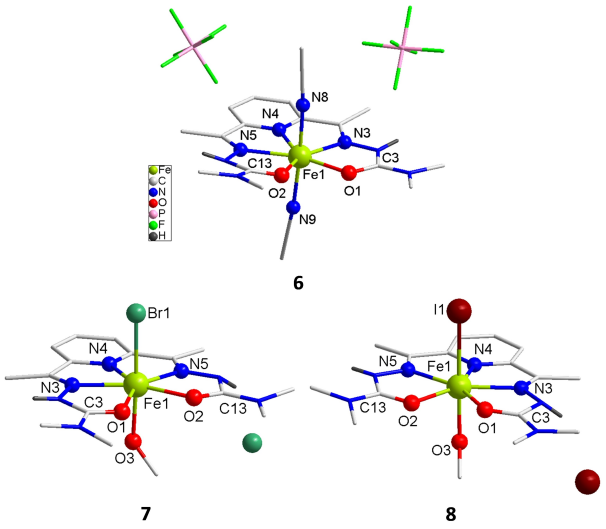

Figure 4. $[FeH_2L^{NMe2}(MeCN)_2]\cdot(PF_6)_2\cdot MeCN$, **6**, $[FeH_2L^{NMe2}(MeOH)Br]\cdot Br$, **7**, and $[FeH_2L^{NMe2}(MeOH)I]\cdot I$, **8**. The lattice solvent molecule (in **6**) and H-atoms are not shown except the H of the N-hydrazide moieties.

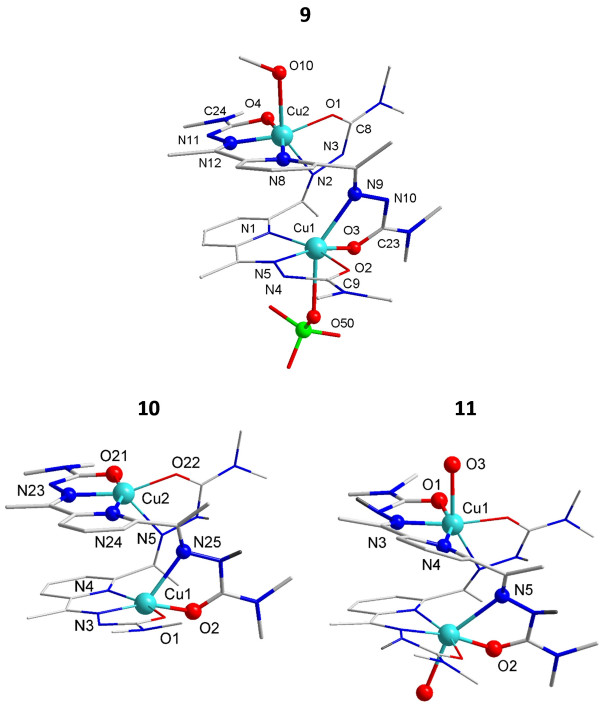

Figure 5. Crystal structures of the molecular complexes in $[\{CuH_2L^{NMe2}\}_2(ClO_4)(MeOH)]\cdot(ClO_4)_3\cdot 1H_2O{\cdot}1.75MeOH$, **9**, $[CuHL^{NMe2}]_2\cdot(ClO_4)_2\cdot H_2O$, **10**, and $[CuH_2L^{NMe2}(H_2O)]_2\cdot(ClO_4)_4\cdot 5H_2O$, **11**. The anions, lattice solvent molecule, and H-atoms are not shown except the H atoms of the N-hydrazide moieties.

Br < I; Fe1-N8 = 2.155 Å (**6**) < Fe1-Br1 = 2.677 Å (**7**) < Fe1-I1 = 2.881 Å (**8**)).

The Cu^{II} derivatives all consist in dinuclear complexes involving two pentadentate ligands wrapped around two Cu^{II} ions (Figure 5).

Complex $[\{CuH_2L^{NMe2}\}_2(MeOH)(ClO_4)]\cdot(ClO_4)_3\cdot 1H_2O{\cdot}1.75$ MeOH, **9**, crystallized in the triclinic space group *P*1 as a dinuclear complex with two distinct hexacoordinate Cu centers. The asymmetric unit comprises two complexes that differ in the direction of the ligand wrapping around the Cu ion (i.e. clockwise or counter-clockwise). The coordination sphere of each Cu^{II} involves two H_2L^{NMe2} ligands in 3 + 2 coordination mode. For each ligand, one O-atom and two nitrogen atoms of the pyridine and one hydrazone occupy three sites of the basal coordination sphere of one Cu center and the remaining O- and N-atoms are linked to the second metal center. This [N_2O + NO] coordination motif between the pentadentate ligands and the Cu^{II} ions is found in the three compounds **9**, **10**, and **11**. The coordination sphere of the Cu centers in **9** is completed to six by respectively one MeOH and one ClO_4^- anion, coordinated by an oxygen atom. The coordination polyhedron of the Cu centers is best described as a strongly distorted octahedron (CShM values versus ideal octahedron are 5.173 for Cu1, 4.850 for Cu2, 5.276 for Cu3, and 3.997 for Cu4). Each dinuclear complex is associated to three ClO_4^- anions and 1 H_2O and 1.75 MeOH solvate molecules.

Complex $[CuHL^{NMe2}]_2\cdot(ClO_4)_2\cdot H_2O$, **10**, crystallized in the monoclinic space group $P2_1/n$ as a dimer with two distinct pentacoordinate Cu centers in a strongly distorted square pyramidal arrangement. The coordination sphere of each Cu^{II} involves two mono-anionic $[HL^{NMe2}]^-$ ligands in the 3 + 2 coordination mode as described before. However, in **10** each ligand is deprotonated once as suggested by the hydrazide N–N–C(O) angles, one showing a value above 110° whereas the second is clearly below (Table 4). The bimetallic complex is

Table 3. Selected bond lengths (Å) and angles (°) for **6**–**8**.

6		**7**		**8**	
Fe1–N5	2.243(3)	Fe1–N5	2.222(2)	Fe1–N3	2.229(3)
Fe1–N4	2.216(3)	Fe1–N4	2.203(2)	Fe1–N4	2. 197(3)
Fe1–N3	2.232(3)	Fe1–N3	2.231(2)	Fe1–N5	2.228(4)
Fe1–O2	2.166(3)	Fe1–O2	2.221(2)	Fe1–O1	2.206(3)
Fe1–O1	2.145(3)	Fe1–O1	2.101(2)	Fe1–O2	2.108(3)
Fe1–N8	2.155(3)	Fe1–Br1	2.676(1)	Fe1–I1	2.881(1)
Fe1–N9	2.194(3)	Fe1–O3	2.191(2)	Fe1–O3	2.170(4)
N8–Fe1–N9	176.1(1)	Br1–Fe1–O3	175.67(6)	I1–Fe1–O3	176.32(9)
N3–N2–C3	113.4(3)	N3–N2–C3	112.4(2)	N3–N2–C3	112.4(3)
N5–N6–C13	112.7(3)	N5–N6–C13	112.0(2)	N5–N5–C13	112.2(3)

Table 4. Selected bond lengths (Å) and angles (°) for **9**–**11**.

9		**10**		**11**	
Cu1–N1	2.046(7)	Cu1–N3	1.925(3)	Cu1–N3	1.954(2)
Cu1–N5	1.927(4)	Cu1–N4	2.043(3)	Cu1–N4	2.070(2)
Cu1–N9	2.322(5)	Cu1–N25	2.304(2)	Cu1–O1	2.014(2)
Cu1–O2	2.036(6)	Cu1–O2	1.969(2)	Cu1–O2	1.940(1)
Cu1–O3	2.829(5)	Cu1–O1	1.988(2)	Cu1–O3	2.333(2)
Cu1–O50	2.474(2)	Cu2–N5	2.291(3)	Cu1–N5	2.450(2)
Cu2–N2	2.338(6)	Cu2–N24	2.052(3)	N5–Cu1–O3	150.83(6)
Cu2–N8	2.045(7)	Cu2–N23	1.923(3)	N3–N2–C3	111.2(2)
Cu2–N12	1.883(8)	Cu2–O21	2.018(3)	N5–N6–C13	115.2(2)
Cu2–O1	1.934(6)	Cu2–O22	1.974(2)		
Cu2–O4	2.04(1)	N3–N2–C3	106.9(3)		
Cu2–O10	2.375(8)	N5–N6–C13	113.3(3)		
N2–N3–C8	112.4(7)	N23–N22–C23	107.8(3)		
N4–N5–C9	110.9(5)	N25–N26–C33	113.1(3)		
N9–N10–C23	113.9(5)				
N12–N11–C24	108(1)				

therefore dicationic and associated to two ClO_4^- anions, one being disordered over two positions. The compound crystallized with one lattice H_2O molecule.

Compound $[CuH_2L^{NMe2}(H_2O)]_2\cdot(ClO_4)_4\cdot 5H_2O$, **11**, crystallized in the *C2/c* monoclinic space group and consists in a binuclear complex of hexacoordinated Cu^{II} centers very similar to that found in **9**. The H_2L^{NMe2} ligands have a $[N_2O+NO]$ coordination to the Cu centers and are neutral as confirmed by the hydrazide N–N–C(O) angles above 110° (Table 4). The sixth coordination site of each Cu ion is occupied by a H_2O located in apical position. The charge of the molecular complex is balanced by four ClO_4^- ions, two of which were found disordered over two positions. Five H_2O molecules per complex complete the crystal lattice.

Powder X-ray diffraction investigations confirmed the phase purities of all the samples (Figure S14).

Magnetic behaviors

The magnetic behaviors for complexes **2**–**8** were studied in order to evaluate a possible effect of the new pentadentate ligand on their magnetic anisotropy. The temperature dependence of the magnetic susceptibility, χ_M, between 2 and 300 K and the field dependence of the magnetization for different temperature between 2 and 8 K were systematically recorded. For Co and Fe derivatives, AC susceptibility behaviors were also investigated. When appropriate, the magnetic anisotropy expressed by the complexes was evaluated by considering a zero-field splitting (ZFS) effect; the axial parameter, *D*, and eventually the rhombic parameter, *E*, were deduced from a simultaneous analysis of the $\chi_M T = f(T)$ and $M = f(H)$ behaviors, using the PHI software.[25]

The $\chi_M T = f(T)$ plot for Cr^{III} complex **2b** (Figure S16) is consistent with a mainly paramagnetic behavior. The $\chi_M T$ product at 300 K is 1.87 $cm^3mol^{-1}K$, in agreement with the Curie contribution for an $S = 3/2$ with $g = 2$. This value remains unchanged as *T* is reduced to about 10 K, and it decreases slightly for lower temperatures to reach 1.75 $cm^3mol^{-1}K$ at 2 K. The field dependence of the magnetization at 2 K is 2.8 μ_B for a field of 5 T. Analysis of these behaviors led to an axial ZFS parameter of $|D| = 1.02 \pm 0.04$ cm^{-1} and $g = 2.00$ but its sign could not be ascertained; the same agreement between calculated and experimental data was found whether the sign of this value was positive or negative. However, theoretical calculations (*vide infra*) suggest a negative *D* for **2**. The *D* obtained is similar to the few reported experimental values for related PBP Cr^{III} complexes.[14–15]

The behaviors for the complexes $[MH_2L^{NMe2}(H_2O)_2]\cdot 2ClO_4$ with $M = Mn^{II}$ (**3**), Co^{II} (**4**), or Ni^{II} (**5**) are shown in Figures 6 and S17. The values found for $\chi_M T$ at 300 K are 4.64, 2.54, and 1.30 $cm^3mol^{-1}K$ respectively, for **3**–**5**, in good agreement with the contributions anticipated for these ions. The Mn^{II} complex shows mainly a Curie behavior, modeling considering intermolecular interaction lead to $g = 2.07$ and $zJ = -0.007 \pm 0.001$ cm^{-1},

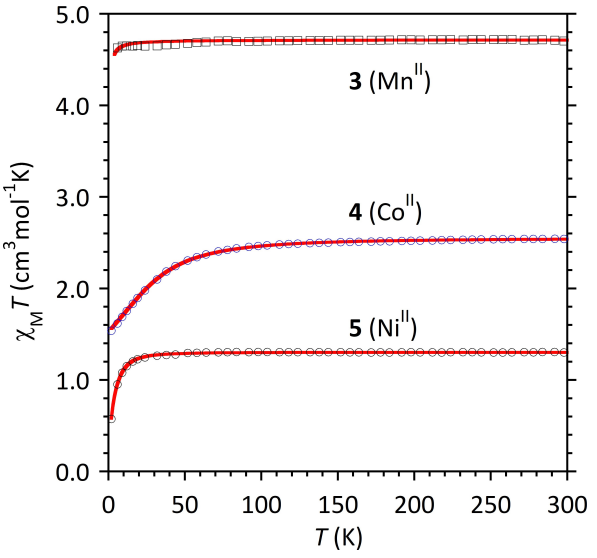

Figure 6. Experimental and calculated (red full lines) $\chi_M T = f(T)$ behaviors for **3**–**5**.

thus supporting the absence of intermolecular exchange interactions. For Co^{II} and Ni^{II} derivatives, a decrease of $\chi_M T$ is observed in the lower T domain in line with the ZFS effect applying for these ions. Modeling of these behaviors gave for **4** $D = 35.6 \pm 0.3\ cm^{-1}$ with $g = 2.33$, and for **5** $D = -14.45 \pm 0.05\ cm^{-1}$, $E = 1.579 \pm 0.009\ cm^{-1}$, and $g = 2.28$. These D values confirm the substantial magnetic anisotropy exhibited by these ions in PBP coordination geometry. The strength and sign of the obtained D parameters are in agreement with reported values for Co^{II} and Ni^{II} in a related coordination environment.[26]

The behaviors for $[FeH_2L^{NMe2}(MeCN)_2]\cdot 2PF_6\cdot MeCN$, **6** (Figure 7), $[FeH_2L^{NMe2}(MeOH)Br]\cdot Br$, **7**, and $[FeH_2L^{NMe2}(MeOH)I]\cdot I$, **8** (Figure S18) are very similar. The values found for $\chi_M T$ in the upper T domain are 3.48, 3.50, and 3.20 $cm^{-1}mol^{-1}K$, respectively, in agreement with an $S = 2$ spin with g slightly larger than 2 as typically found in related PBP derivatives.[27–28] These values hardly change as temperature is reduced to about 50 K, and, for lower temperatures, $\chi_M T$ decreases sharply to 2.68 and 2.93 $cm^{-1}mol^{-1}K$ respectively, for **6** and **7**. Complex **8** shows a similar decrease in $\chi_M T$, but below 5 K a slight rise is detected, which was observed for different samples from different syntheses. As a movement of crystallites under the effect of the field can be excluded because they are blocked in grease or benzene, the origin of this behavior must be attributed to intermolecular interactions. The magnetizations recorded at 2 K reach respectively 2.34 μ_B, 2.86 μ_B, and 2.50 μ_B for an applied field of 50 kOe, significantly below the expected saturation for an $S = 2$ thus underlining substantial ZFS effect for the Fe^{II} centers. Simultaneous analysis of the $\chi_M T = f(T)$ and $M = f(H)$ behaviors for each derivative gave, for **6** $D = -11.4 \pm 0.4\ cm^{-1}$, $zJ' = 0.030 \pm 0.004\ cm^{-1}$, and $g = 2.12$; for **7** $D = -5.9 \pm 0.2\ cm^{-1}$, $zJ' = 0.030 \pm 0.002\ cm^{-1}$, and $g = 2.16$; and for **8** $D = -7.3 \pm 0.3\ cm^{-1}$, $zJ' = 0.047 \pm 0.004\ cm^{-1}$, $g = 2.05$. For all these complexes the magnetic anisotropy is characterized by a negative D value as anticipated for high-spin Fe^{II} in PBP geometry. The differences observed can be ascribed to the ligands in the apical positions that act on the relative energy levels of the d_{xz} and d_{yz} orbitals of the Fe, and thus on D.[28] When the coordinated atom has a symmetric overlap with these orbitals their energy difference is small and $|D|$ is large whereas a dissymmetric interaction splits the energy levels resulting in a smaller $|D|$. The former situation is found for halide ligands or nitrogen-coordinated nitrile/cyanido ligands and the latter for ligands bound to the metal center by an oxygen (i.e. H_2O, ROH), which is the case for **6** and **7**–**8**, respectively. Thus, the differences in the magnetic anisotropy parameters for these compounds are directly correlated to the type of ligand in the apical positions.

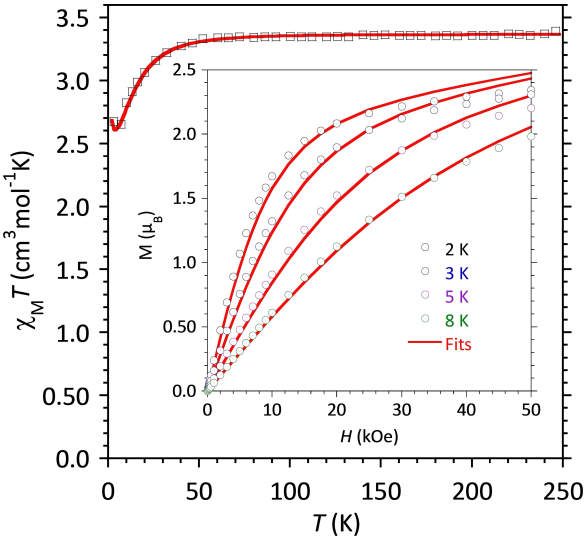

Figure 7. Temperature dependence of $\chi_M T$ and (insert) field dependence of the magnetizations for $[FeH_2L^{NMe2}(MeCN)_2]\cdot 2PF_6\cdot MeCN$, **6** (solid lines are best fits).

AC magnetic susceptibility investigations revealed an out-of-phase component, χ_M'', for $[CoH_2L^{NMe2}(H_2O)_2]\cdot 2ClO_4$, **4**, and for $[FeH_2L^{NMe2}(MeCN)_2]\cdot 2PF_6$, **6**, when applying a static magnetic field. For Co derivative, **4**, the optimal applied field was found to be 2 kOe (Figure S19) and AC susceptibility behavior was recorded in the frequency range 1–1500 Hz. The frequency dependence behavior exhibited by this compound is typical for slow relaxation of the magnetization (Figure 8 and S19). The relaxation times, τ, were assessed by analyzing the $\chi_M'' = f(\nu)$ behaviors with an extended Debye model.[29] The resulting $1/\tau = f(T)$ behavior (Figure 8b) was perfectly reproduced with a model comprising a Raman and a direct relaxation, i.e. $1/\tau = RT^n + AH^2T$. Best fit parameters are $R = 4 \pm 2\ K^{-n}s^{-1}$, $n = 3.7 \pm 0.2$, $A = 33 \pm 5 \times 10^{-6}\ K^{-1}s^{-1}Oe^{-2}$. Such field-induced slow relation of the magnetization governed by Raman and direct relaxation processes are often found in PBP Co^{II} complexes with large positive D.[3] It is attributed to the van Vleck cancellation mechanism.[30]

The optimal applied field for $[FeH_2L^{NMe2}(MeCN)_2]\cdot 2PF_6$, **6**, was found to be 750 Oe (Figure S20) and AC behaviors was recorded with this applied field; a plot of $\chi_M'' = f(\nu)$ between 2 and 4 K is shown in Figure 9 with the deduced relaxation times. The temperature dependence of τ was best modeled using Raman equation (see above) with best fit parameters $R = 546 \pm 16\ K^{-n}s^{-1}$, $n = 2.37 \pm 0.03$.

Theoretical calculations

Ab initio calculations have been performed on compounds **1**, **2b**, **4**, **5**, **6**, **7** and **8** in order to determine the nature and magnitude of the magnetic anisotropy of the metal ions and to find the orientation of the magnetic axes. The method[31] used to evaluate the magnetic anisotropy parameters D and E was described extensively,[7,32–37] therefore only the main aspects are reported in the Computational Information section. Results are reported in Table 5 while the magnetic axes are pictured in Figures 10 and S21. The contribution to the D and E parameters provided by the most contributing excited states are given in Table S4. As usual, it is possible to rationalize the magnitude and nature of the ZFS using perturbative energetic contribution of each excited states and the simple spin-orbit coupling (SOC) operator $\zeta \sum_i (l_i^z s_i^z + (l_i^+ s_i^- + l_i^- s_i^+)/2)$ where ζ is the spin-orbit coupling constant of the free ion. When an excited state and ground state are of same spin and are coupled through the $l_z s_z$ part of the SOC operator, the contribution is negative. If their

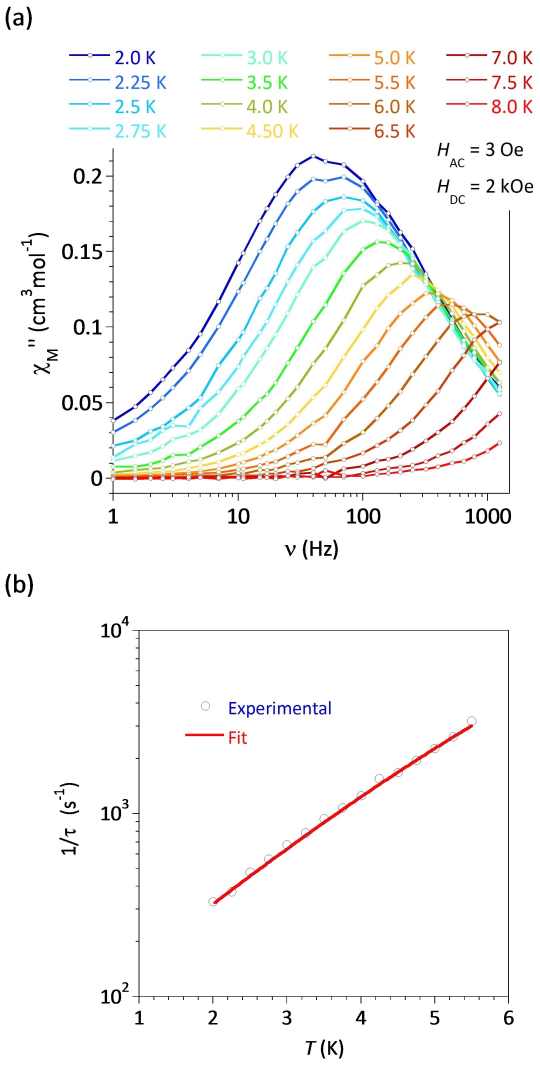

Figure 8. $[CoH_2L^{NMe2}(H_2O)_2]\cdot 2ClO_4$, **4**: (a) $\chi_M''=f(\nu)$ behaviors between 2 and 8 K with $H_{DC}=2$ kOe, (b) $1/\tau=f(T)$ with best fit (red line) of an expression for Raman and direct relaxations.

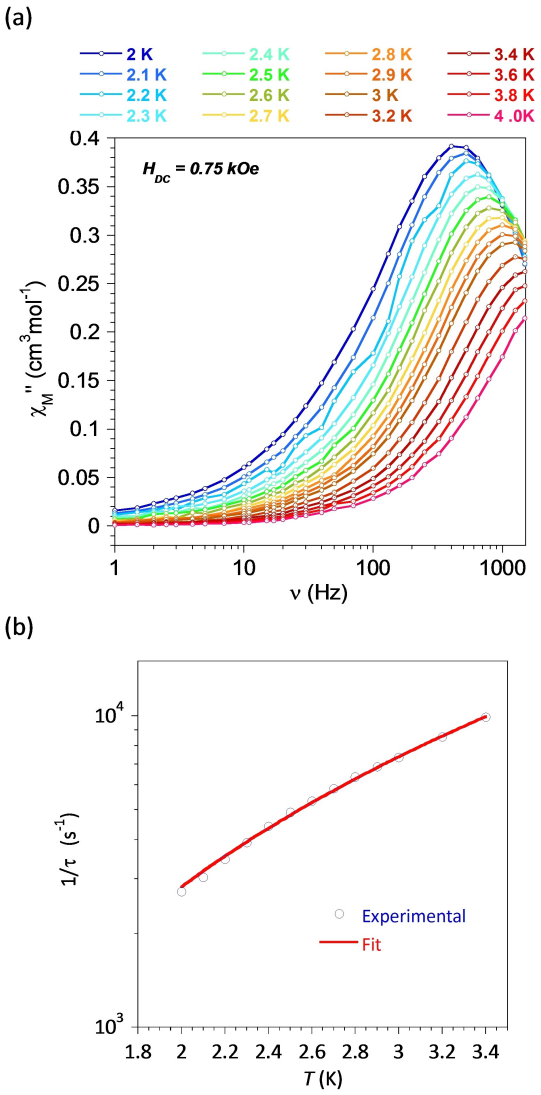

Figure 9. $[FeH_2L^{NMe2}(MeCN)_2]\cdot 2PF_6$, **6**: (a) $\chi_M''=f(\nu)$ behaviors between 2 and 4 K with $H_{DC}=0.75$ kOe, (b) $1/\tau=f(T)$ with best fit (red line) of an expression for Raman relaxation.

Table 5. Experimental and calculated ZFS parameters (in cm^{-1}) and g values for compounds **1**, **2b**, **4**, **5**, **6**, **7**, and **8**. The lines marked [a] and [b] correspond respectively to complexes whose nearest halide anion has, or has not, been explicitly introduced in the calculations (see text).

	Experimental			Calculated						
	D	g_{iso}		D	E/D	E	g_x	g_y	g_z	g_{iso}
1	–	–		−1.57	0.12	−0.19	1.96	1.96	1.93	1.95
2b	|1.02|	2.00		−1.22	0.23	−0.28	1.97	1.97	1.94	1.96
4	35.6	2.33		36.42	0.03	1.13	2.31	2.34	2.02	2.23
5	−14.45	2.28		−17.79	0.10	−1.74	2.26	2.26	2.36	2.28
	$E=1.58$									
6	−11.4	2.12		−14.69	0.12	−2.04	2.05	2.05	2.36	2.13
7	−5.9	2.16	[a]	−7.97	0.33	2.61	2.09	2.09	2.25	2.12
			[b]	7.28	0.24	1.72	2.09	2.21	2.02	2.11
8	−7.3	2.05	[a]	−9.62	0.27	2.39	2.08	2.01	2.27	2.12
			[b]	7.72	0.33	2.56	2.08	2.24	2.01	2.11

spins differ by 1 then the $l_z s_z$ coupling brings a positive contribution. Conversely, for two states of same spin, a coupling through $(l^+s^- + l^-s^+)/2$ generates a positive contribution to D, but if their spin is different, this coupling provides a negative

contribution. Let us recall that the d_{xy} and $d_{x^2-y^2}$ orbitals are linear combinations of the d_{2-} to the d_{2+} spherical harmonics, d_{xz} and d_{yz} are linear combinations of the d_{1-} to the d_{1+} and $d_{z^2} = d_0$. Then, l_z may couple d_{xy} with $d_{x^2-y^2}$ or d_{xz} with d_{yz} and l^+ and l^- may couple d_{xz} and d_{yz} with either d_{xy}, $d_{x^2-y^2}$ or d_{z^2}.

As expected in PBP geometry, the axial parameter D is negative for the Ni complex, **5** (Table 5). The main determinant of the ground state is $\left|d_{xz}\overline{d_{xz}}d_{yz}\overline{d_{yz}}\ d_{x^2-y^2}\ \overline{d_{x^2-y^2}}d_{xy}\ d_{z^2}\right|$. The three first triplet and the third singlet excited states play the most important role. The first triplet that is obtained by an excitation from the $d_{x^2-y^2}$ to d_{xy} orbitals therefore generates a negative contribution to D. The second and third excited triplets are obtained by excitations from d_{xz} and d_{yz} to d_{z^2} respectively, generating a positive contribution to D. The open-shell singlet essentially carried by the configuration $d^2_{xz}d^2_{yz}d^2_{xy}\ d^1_{x^2-y^2}d^1_{Z^2}$ brings a positive contribution as it is coupled through the l_zs_z operator to the ground state. As these three last excited states are much higher in energy than the first one, the overall contribution is negative.

For Co^{II} complex **4**, the anticipated positive value of the D parameter was indeed obtained. The main determinant of the ground state is $\left|d_{xz}\overline{d_{xz}}d_{yz}\overline{d_{yz}}\ d_{x^2-y^2}\ d_{xy}\ d_{z^2}\right|$. The third and fourth excited quartet states contribute positively to D as they are obtained by excitations from the d_{xz} and d_{yz} orbitals to the $d_{x^2-y^2}$ one. The fourth excited doublet state is obtained by an excitation from the d_{xy} to the $d_{x^2-y^2}$ orbitals. Because it has a different spin than the ground state, its contribution is also positive. Unlike the Ni complex where the contributions were opposite, here all the contributions add up to a very large D value.

For the Cr^{III} complexes, **1** and **2b**, the main determinant of the ground state is $\left|d_{xz}d_{yz}\ d_{xy}\right|$. The same physics governs the anisotropy of both complexes. Only the first excited quartet and the fifth doublet contribute significantly to the ZFS. The first quartet obtained through the excitation from the d_{xy} to the $d_{x^2-y^2}$ orbitals contributes negatively. The fifth doublet is a three-open-shell state mainly carried by the configuration $d^1_{xz}d^1_{yz}d^1_{x^2-y^2}$. It therefore brings a positive value. As the two contributions are of comparable magnitude but opposite sign, the resulting value of D is low.

The wave function for Fe^{II} complex **6**, is dominated by the determinant $\left|d_{xz}d_{yz}\overline{d_{yz}}\ d_{x^2-y^2}\ d_{xy}\ d_{z^2}\right|$. This determinant is coupled through l_zs_z with the first excited quintet state that is dominated by the determinant $\left|d_{xz}\overline{d_{xz}}d_{yz}\ d_{x^2-y^2}\ d_{xy}\ d_{z^2}\right|$. The contribution is therefore negative. Several other excited states bring a small contribution, sometimes positive, sometimes negative, rationalizing the final value obtained. We will not specify them here for reasons of simplicity. However, the same reasoning as above applies and allows to explain the nature of each of them. For complexes **7** and **8**, the $|E/D|$ value is very close the undetermined case ($|E/D| = 1/3$) where the D and E values cannot be determined. In such a situation, the slightest geometrical or electrostatic change can make D change from positive to negative, *i.e.* swap the axes of easy and hard magnetization. In order to improve our description, we have introduced the closest halide anion (either Br^- or I^-) explicitly in the calculation (in addition to the coordinated halide that is always considered). As a result, the value of D changes from positive to negative and the y and z axis of the ZFS tensor permute (see Tables 5 and S4, and Figure 10). The main effect of this intermolecular interaction is the rotation of the OH bond of the coordinated MeOH in the direction of the halide and the formation of an H-bond, which probably changes slightly the ligand field in the first coordination sphere (we recall that the position of the H-atoms was optimized, see computational details). For these calculations, the analysis of the contributions to D is the same as that given for complex **6**.

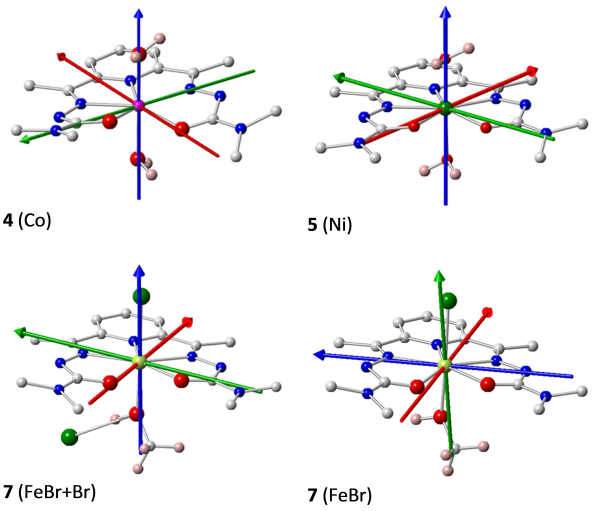

Figure 10. Computed magnetic axes (x is red, y is green and z is blue) for the **4** (Co^{II}), **5** (Ni^{II}), and **7** (Fe^{II}). The role of H-bonded X^- counter-anion (FeBr + Br) and without (FeBr) is illustrated for **7**.

It may be noted from Figure 10 that the z-axis is nearly aligned along the metal-L_{axial} bonds (*i.e.* perpendicular to the equatorial plane) for all complexes except complex **7** in absence of the closest halide, for which *ab initio* calculations predict a positive D value.

Concluding Remarks

The information gathered on the metal complexes formed with H_2L^{NMe2} confirms that the NMe_2 substituents in the hydrazide moieties do not alter the ability of the ligand to stabilize the PBP coordination arrangement. Referring to the shorter bond lengths, it appears that the metal-ligand interactions are among the strongest known for this H_2L^R ligand family. This is likely related to the increased donor character of the dimethylamino groups. As a result, the equatorial ligand field must be larger.

However, the magnetic anisotropy found for the Co^{II} and Fe^{II} complexes are very similar to that known for related PBP derivative, confirming the ligand H_2L^{NMe2} has no major effect on these magnetic characteristics. *Ab initio* calculations confirm the values of the ZFS parameters extracted from magnetic measure-

ments. Analyses of the wave functions rationalize the magnitude and nature of the ZFS. One may note, that for complexes **7** and **8**, the value of $|E/D|$ is very close to 1/3 and that this makes them very versatile compounds, likely to exhibit axial or planar magnetic anisotropy.

Finally, the metal complexes formed with H_2L^{NMe2} exhibit good solubility in a wide range of solvents compared to the classically used H_2L^R ligands with $R = NH_2$, aryl, or alkyl. They also proved to be quite easy to crystallize.

Supporting Information Summary

The supporting information contains the experimental details, synthesis procedures and analytical information, crystallographic and geometric information; NMR; IR, and PXRD plots; additional magnetic data.

CCDC: Deposition Numbers 2182419 (**K_2L**); 2182420 (**1**); 2182415 (**2a**); 2182421 (**2b**); 2182422 (**3**); 2182414 (**4**); 2182423 (**5**); 2182417 (**6**); 2182416 (**7**); 2182424 (**8**); 2225500 (**9**), 2182418 (**10**); 2182425 (**11**) contain the supplementary crystallographic data for this paper. These data are provided free of charge by the joint Cambridge Crystallographic Data Centre and Fachinformationszentrum Karlsruhe Access Structures service.

Acknowledgements

This work was supported by the French National Research Agency, ANR, (grant ANR-17-CE07-0007). Authors are grateful to M. J.-F. Meunier (LCC) for technical assistance in magnetic data collections.

Conflict of Interest

The authors declare no conflict of interest.

Data Availability Statement

The data that support the findings of this study are available from the corresponding author upon reasonable request.

Keywords: ab initio calculations · heptacoordination · magnetic anisotropy · N,O ligands · pentagonal bipyramidal;

[1] A. K. Bar, C. Pichon, J.-P. Sutter, *Coord. Chem. Rev.* **2016**, *308*, 346–380.
[2] S. Gómez-Coca, D. Aravena, R. Morales, E. Ruiz, *Coord. Chem. Rev.* **2015**, *289–290*, 379–392.
[3] J.-P. Sutter, V. Béreau, V. Jubault, K. Bretosh, C. Pichon, C. Duhayon, *Chem. Soc. Rev.* **2022**, *51*, 3280–3313.
[4] T. S. Venkatakrishnan, S. Sahoo, N. Bréfuel, C. Duhayon, C. Paulsen, A.-L. Barra, S. Ramasesha, J.-P. Sutter, *J. Am. Chem. Soc.* **2010**, *132*, 6047–6056.
[5] D. Shao, S.-L. Zhang, X.-H. Zhao, X.-Y. Wang, *Chem. Commun.* **2015**, *51*, 4360–4363.
[6] V. D. Sasnovskaya, V. A. Kopotkov, A. D. Talantsev, R. B. Morgunov, E. B. Yagubskii, S. V. Simonov, L. V. Zorina, V. S. Mironov, *Inorg. Chem.* **2017**, *56*, 8926–8943.
[7] C. Pichon, N. Suaud, C. Duhayon, N. Guihéry, J.-P. Sutter, *J. Am. Chem. Soc.* **2018**, *140*, 7698–7704.
[8] B. Drahoš, R. Herchel, Z. Trávníček, *Inorg. Chem.* **2018**, *57*, 12718–12726.
[9] L. V. Zorina, S. V. Simonov, V. D. Sasnovskaya, A. D. Talantsev, R. B. Morgunov, V. S. Mironov, E. B. Yagubskii, *Chem. Eur. J.* **2019**, *25*, 14583–14597.
[10] K. Bretosh, V. Béreau, C. Duhayon, C. Pichon, J.-P. Sutter, *Inorg. Chem. Front.* **2020**, *7*, 1503–1511.
[11] C. Pichon, C. Duhayon, E. Delahaye, J.-P. Sutter, *Eur. J. Inorg. Chem.* **2021**, *2021*, 5112–5118.
[12] V. Jubault, *Ph.D. Thesis*, University of Toulouse (France), **2022**.
[13] A. Bino, R. Frim, M. Van Genderen, *Inorg. Chim. Acta* **1987**, *127*, 95–101.
[14] C. Pichon, B. Elrez, V. Béreau, C. Duhayon, J.-P. Sutter, *Eur. J. Inorg. Chem.* **2018**, *2018*, 340–348.
[15] T. A. Bazhenova, L. V. Zorina, S. V. Simonov, Y. V. Manakin, A. B. Kornev, K. A. Lyssenko, V. S. Mironov, I. F. Gilmutdinov, E. B. Yagubskii, *Inorg. Chim. Acta* **2021**, *522*, 120358.
[16] I. Suzuki, J. Nakagawa, T. Fujiyama, *Spectrochim. Acta Part A* **1977**, *33*, 689–698.
[17] M. Llunell, D. Casanova, J. Cirera, P. Alemany, S. Alvarez, *in SHAPE: Program for the stereochemical analysis of molecular fragments by means of continuous shape measures and, associated tools, Vol.* University of Barcelona, Barcelona, **2013**.
[18] S. Alvarez, P. Alemany, D. Casanova, J. Cirera, M. Llunell, D. Avnir, *Coord. Chem. Rev.* **2005**, *249*, 1693–1708.
[19] D. Casanova, P. Alemany, J. M. Bofill, S. Alvarez, *Chem. Eur. J.* **2003**, *9*, 1281–1295.
[20] S. Alvarez, M. Llunell, *Dalton Trans.* **2000**, *29*, 3288–3303.
[21] N. Gogoi, M. Thlijeni, C. Duhayon, J.-P. Sutter, *Inorg. Chem.* **2013**, *52*, 2283–2285.
[22] B. Drahoš, R. Herchel, Z. Trávníček, *Inorg. Chem.* **2015**, *54*, 3352–3369.
[23] M. Dey, P. P. Mudoi, A. Choudhury, B. Sarma, N. Gogoi, *Chem. Commun.* **2019**, *55*, 11547–11550.
[24] Y.-F. Deng, B. Yao, P.-Z. Zhan, D. Gan, Y.-Z. Zhang, K. R. Dunbar, *Dalton Trans.* **2019**, *48*, 3243–3248.
[25] N. F. Chilton, R. P. Anderson, L. D. Turner, A. Soncini, K. S. Murray, *J. Comput. Chem.* **2013**, *34*, 1164–1175.
[26] R. Ruamps, L. J. Batchelor, R. Maurice, N. Gogoi, P. Jiménez-Lozano, N. Guihéry, C. de Graaf, A.-L. Barra, J.-P. Sutter, T. Mallah, *Chem. Eur. J.* **2013**, *19*, 950–957.
[27] A. K. Bar, C. Pichon, N. Gogoi, C. Duhayon, S. Ramasesha, J.-P. Sutter, *Chem. Commun.* **2015**, *51*, 3616–3619.
[28] A. K. Bar, N. Gogoi, C. Pichon, V. M. L. D. P. Goli, M. Thlijeni, C. Duhayon, N. Suaud, N. Guihéry, A.-L. Barra, S. Ramasesha, J.-P. Sutter, *Chem. Eur. J.* **2017**, *23*, 4380–4396.
[29] C. Dekker, A. F. M. Arts, H. W. de Wijn, A. J. van Duyneveldt, J. A. Mydosh, *Phys. Rev. B* **1989**, *40*, 11243.
[30] S. Gómez-Coca, A. Urtizberea, E. Cremades, P. J. Alonso, A. Camón, E. Ruiz, F. Luis, *Nat. Commun.* **2014**, *5*, 5300.
[31] R. Maurice, R. Bastardis, C. d. Graaf, N. Suaud, T. Mallah, N. Guihéry, *J. Chem. Theory Comput.* **2009**, *5*, 2977–2984.
[32] C. Pichon, N. Suaud, V. Jubault, C. Duhayon, N. Guihéry, J.-P. Sutter, *Chem. Eur. J.* **2021**, *27*, 15484–15495.
[33] M. Rubín-Osanz, F. Lambert, F. Shao, E. Rivière, R. Guillot, N. Suaud, N. Guihéry, D. Zueco, A.-L. Barra, T. Mallah, F. Luis, *Chem. Sci.* **2021**, *12*, 5123–5133.
[34] F. El-Khatib, B. Cahier, M. López-Jordà, R. Guillot, E. Rivière, H. Hafez, Z. Saad, N. Guihéry, T. Mallah, *Eur. J. Inorg. Chem.* **2018**, *2018*, 469–476.
[35] G. Novitchi, S. Jiang, S. Shova, F. Rida, I. Hlavička, M. Orlita, W. Wernsdorfer, R. Hamze, C. Martins, N. Suaud, N. Guihéry, A.-L. Barra, C. Train, *Inorg. Chem.* **2017**, *56*, 14809–14822.
[36] F. El-Khatib, B. Cahier, F. Shao, M. López-Jordà, R. Guillot, E. Rivière, H. Hafez, Z. Saad, J.-J. Girerd, N. Guihéry, T. Mallah, *Inorg. Chem.* **2017**, *56*, 4601–4608.
[37] B. Cahier, R. Maurice, H. Bolvin, T. Mallah, N. Guihéry, *Magnetochemistry* **2016**, *2*, 31.

Submitted: December 20, 2022
Accepted: January 5, 2023